



Supplement of

Significant response of methane in the upper troposphere to subseasonal variability in the Asian monsoon anticyclone

Sihong Zhu et al.

Correspondence to: Mengchu Tao (mengchutao@mail.iap.ac.cn)

The copyright of individual parts of the supplement might differ from the article licence.

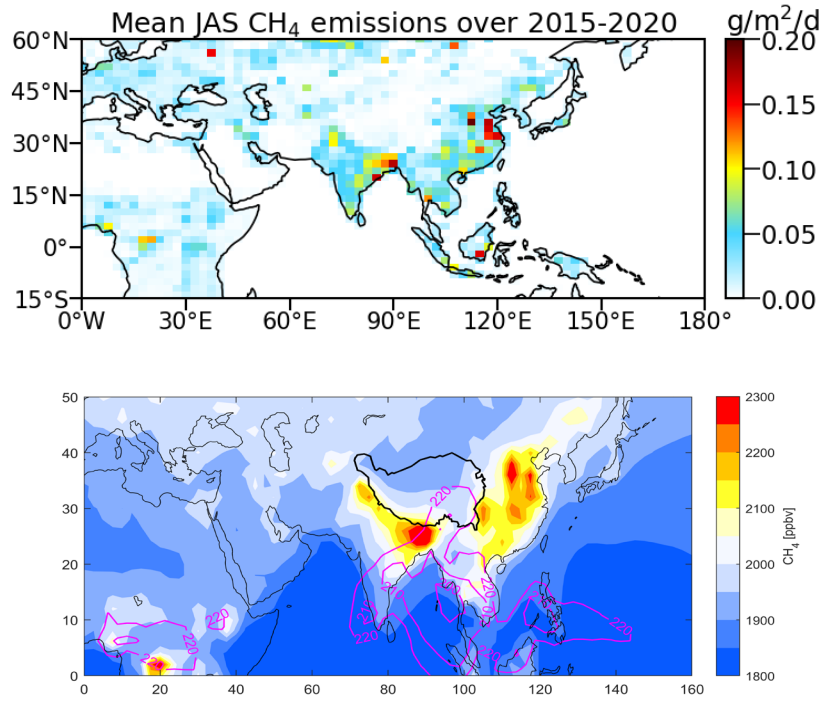


Figure S1: Map of mean CH₄ emission flux (top panel, unit: g/m²/day) and near-surface CH₄ volume mixing ratios at lowest model level (bottom panel, unit: ppbv) during the JAS season (July–September) averaged over 2015–2020. The magenta contours indicate outgoing longwave radiation (OLR) lower than 220 K for each mode, with an interval of 10 K, which represents the deep convective cloud.

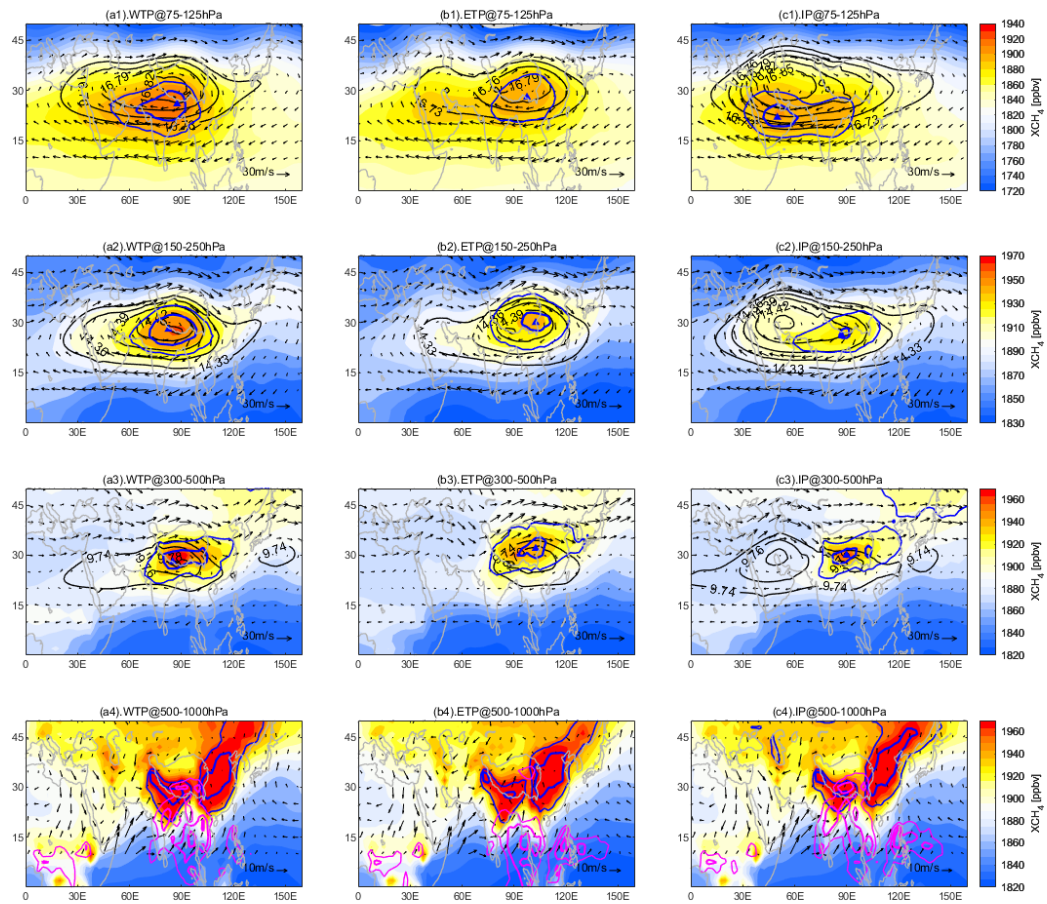


Figure S2: Horizontal distribution of composites XCH_4 concentration corresponding to the three dominant AMA modes, shown across four vertical layers: the lowermost stratosphere (75–125 hPa; top panels a1–c1), the upper troposphere (150–250 hPa; panels a2–c2), the middle troposphere (300–400 hPa; panels a3–c3), and the lower troposphere (500–1000 hPa; bottom panels a4–c4). Color shading indicates the XCH_4 at each pressure layer. Black contours depict the GPH field outlining the AMA structure. Blue lines enclose regions with high occurrence frequencies (50% and 70%) of elevated methane—defined as in Figure 3—and triangles mark the locations with highest occurrence frequency.

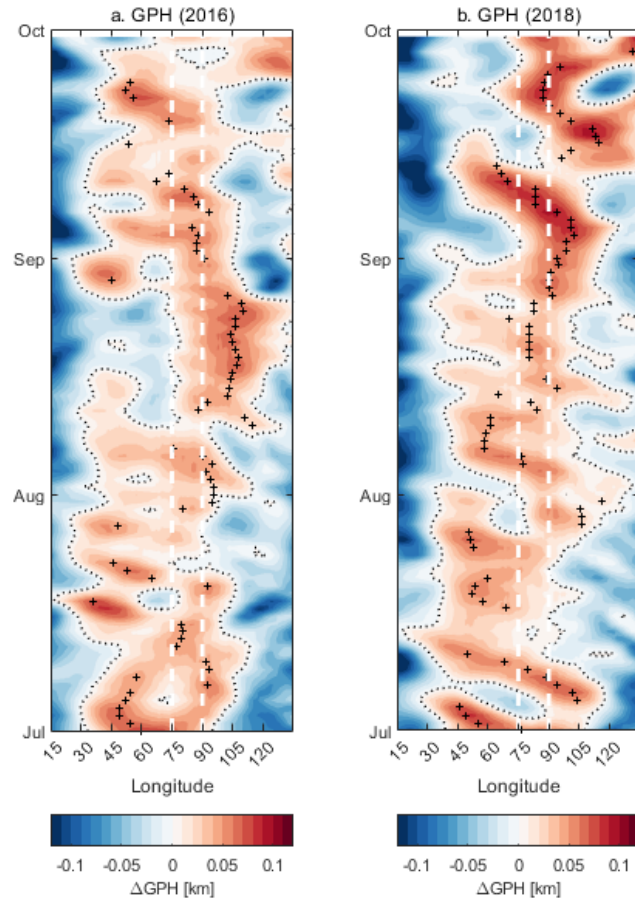


Figure S3: Hovmöller diagram of geopotential height for 2016 and 2018 JAS. The black crosses show the position of AMA center. The white dashed lines show the latitude range (75-90°E) for WTP mode.

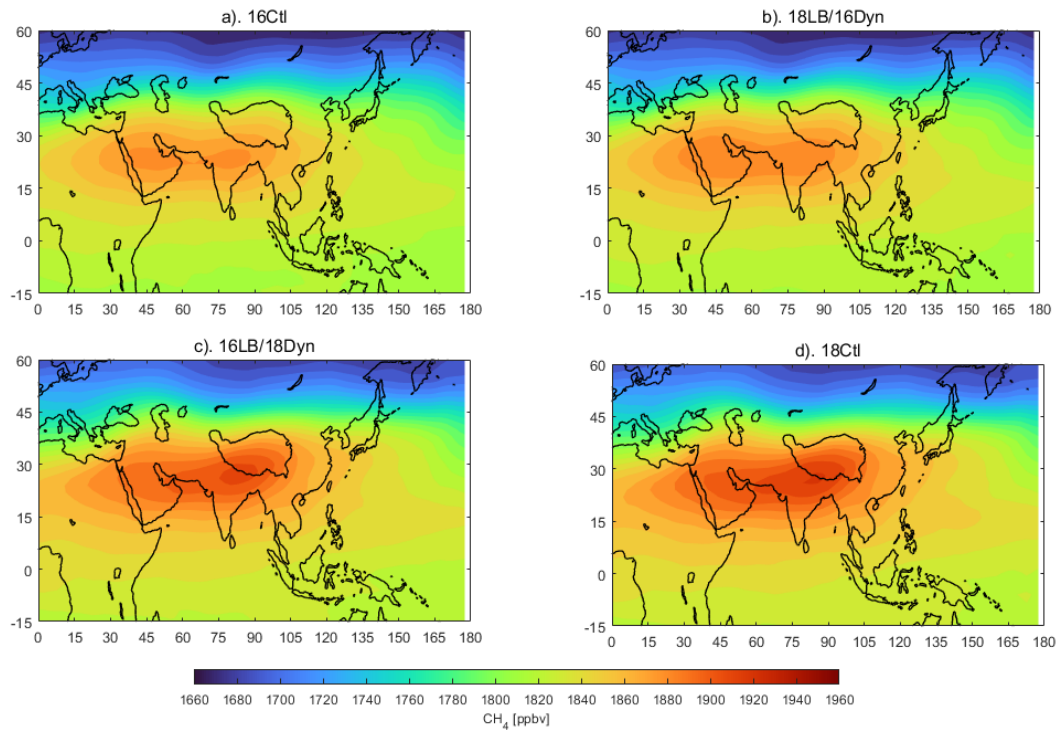


Figure S4: The mean CH_4 distribution during JAS at 100hPa based on 4 test runs for the year 2016 and 2018 listed at Table 1 (fixed L.B. runs).

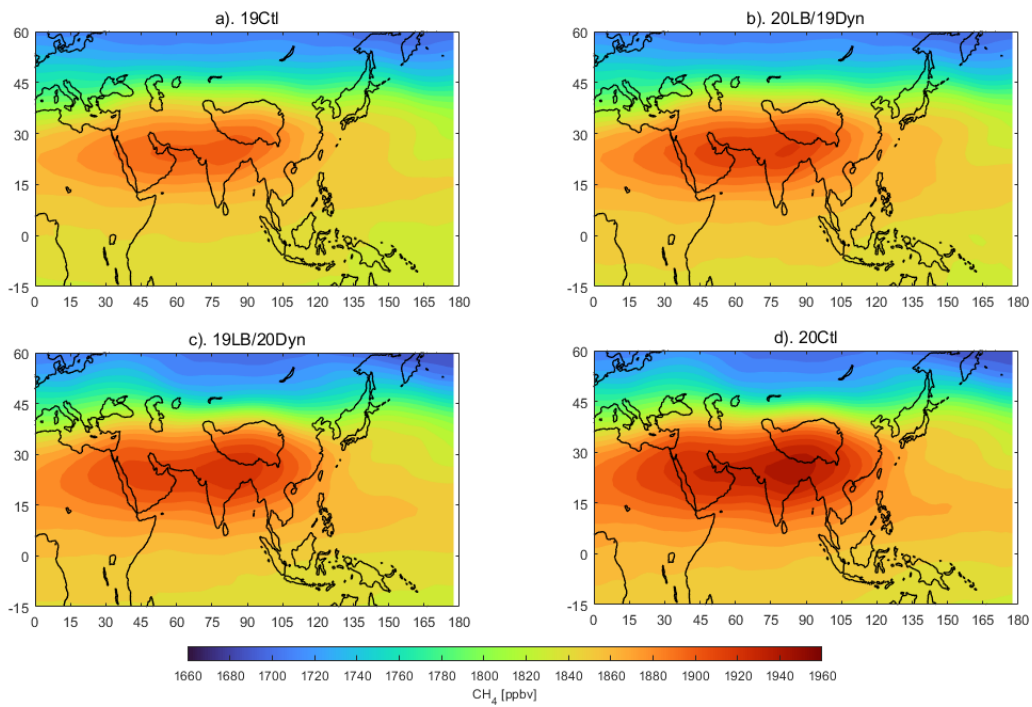


Figure S5: The mean CH_4 distribution during JAS at 100hPa based on 4 test runs for the year 2019 and 2020 listed at Table 1 (fixed Dyn. Runs).

As we can see in Figure S3 and S4, the mean CH_4 distribution at 100hPa over ASM region are not sensitive to the shift of boundary condition but more sensitive to change in the dynamical configuration.

Moreover, in Figure S3, we find that difference between 16LB/18Dyn (c) and 16Ctl (a) are almost identical to the difference between 18Ctl (d) and 18LB/16Dyn (b). So are the corresponding difference shown in Figure S4.

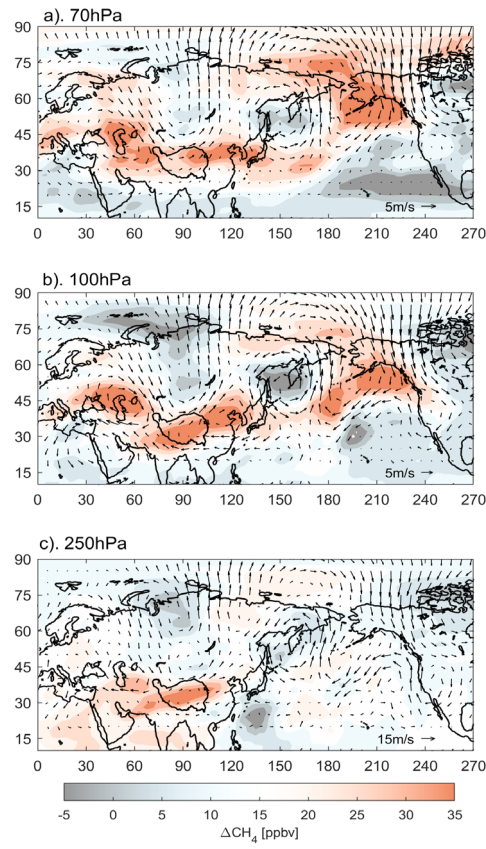


Figure S6: Similar as Fig. 6 (b1-3) but for larger spatial range. The arrows indicate the differences in horizontal wind between the dynamical fields of 2016 and 2018.